International Journal of Applied Electromagnetics and Mechanics 46 (2014) 693–708
DOI 10.3233/JAE-141966
IOS Press

A comparison between the epoxy-bonded layer structure and shear-lag model in a thickness-shear mode circular cylindrical piezoelectric transformer

Peng Li and Feng Jin*
State Key Laboratory for Strength and Vibration of Mechanical Structures, School of Aerospace, Xi'an Jiaotong University, Xi'an, Shaanxi, China

Abstract. The thickness-shear modes in a circular cylindrical piezoelectric transformer considering the effect of an epoxy-bonded layer are analyzed, and an exact solution is obtained from the equations of the linear theory of piezoelectricity. Systematic parametric studies are subsequently carried out to quantify the effects of the epoxy-bonded layer upon the transformer performance, including its thickness, elastic coefficient and mass density. It is demonstrated that whilst the thickness and elastic coefficient of the layer affect significantly the resonance frequencies, transforming ratio, power density, admittance and efficiency, and its mass density has negligible influence. On condition that the thickness of the epoxy layer is vanishingly small so that it degenerates into the solution by the classical shear-lag model. Upon comparing with the predictions obtained by employing the traditional shear-lag model, it is found that the interface viscous damping is absolutely due to the elastic coefficient of the epoxy layer, and the present structure model is found to be more accurate especially when the thickness of the epoxy layer can not be neglected.

Keywords: Thickness-shear mode, cylindrical piezoelectric transformer, epoxy-bonded layer, shear-lag model, viscous damping

1. Introduction

As a class of smart structures, piezoelectric transformer has been successfully made into many electronic devices, such as computer backlights, florescent ballast, portable electronic chargers, ignition of gas-discharge lamps, and compact ac/dc and dc/dc converters, etc., which are used to raise or lower a voltage [1–3]. All of these devices are based on the strong coupling property between electric and mechanical constitutive behavior. Many transformer investigations have been carried on theoretically and experimentally [4–7], and more other references can be found in a review article [8]. Most of the work is focused on perfect bonding. To the authors' best knowledge, few work has been carried out so far to discuss the effect of imperfect interface on the behavior of a piezoelectric transformer. However, it has been recently pointed out that imperfect bonding does exists in devices, and this is significant for

*Corresponding author: Feng Jin, State Key Laboratory for Strength and Vibration of Mechanical Structures, School of Aerospace, Xi'an Jiaotong University, Xi'an 710049, Shaanxi, China. Tel./Fax: +86 29 8266 7091; E-mail: jinfengzhao@263.net.

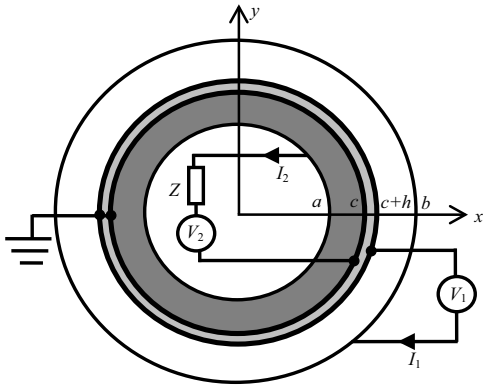

Fig. 1. A cylindrical piezoelectric ceramic transformer with an epoxy-bonded layer.

the design of high quality electronic devices. Therefore, the present contribution is concentrated on the influence investigation of imperfect interface in piezoelectric transformers.

The transformers mentioned above contain at least two working components, i.e., input and output parts. Very often a gluing substance, e.g., epoxy, is applied to connect the two portions and form an interface [9]. Sometimes, micro-defect, diffusion impurity and damage take place inevitably during the production of these devices, which will lead to the imperfectly bonded interface at the joint. Besides, the interface may be damaged under harsh conditions, which would in turn affect the electromechanical behaviors of the piezoelectric sensors [10]. For instance, compared with the perfectly bonded case, the imperfect interface can lower the frequency of the resonator [11], induce the localization of some particular waves [12], make the material distribution around the joint inhomogeneous [10], change the wave dispersion properties [13], and so on.

Researchers have developed imperfect interface models with different levels of sophistication [11–16]. The simplest description is to treat it as a layer which possesses elasticity and interface elastic strain energy, but geometrically has a zero thickness, e.g., a shear-lag model [13–15]. Mechanical and electrical properties and behaviors of weak interfaces described by different models have been widely studied theoretically [13–16] and experimentally [17,18]. More references about the imperfect interface can be found in a few review articles [19,20]. It has been proved that an interphase or transition with thickness typically in the range of 30–240 nm does exist across the interface [21,22]. However, the references which have ignored the thickness of the interface layer may produce unavoidable error, especially for the smart structures with only several micro-meters thick. The accuracy of the model predictions has therefore an issue of concern, although this is yet quantified.

In the present study, an epoxy-bonded layer structure is proposed for investigating the effect of an epoxy layer on the thickness-shear modes in a circular cylindrical piezoelectric transformer. Built upon the solutions obtained, the effects of the thickness, elastic coefficient and mass density of the epoxy layer are quantified. Subsequently, with the assumption that the thickness of the middle layer is vanishingly small, the epoxy-bonded layer structure is used to characterize piezoelectric transformers having imperfectly bonded interfaces. Finally, the present model predictions are compared with those obtained using the traditional shear-lag model and some conclusions can be drawn.

2. Theoretical analysis of the cylindrical piezoelectric transformer with an epoxy layer

Consider a piezoelectric circular cylinder of polarized ceramics (see Fig. 1) with the z axis being the

poling direction or the six-fold axis. Usually, the epoxy glue is used to splice two different portions. For instance, Wu et al. have used the epoxy glue to made copper-layer and aluminum-substrate SAW devices [9,23]. Here we assume that this epoxy bonded layer exists at $r = c$ with its thickness h. The piezoelectric ceramics is unbounded in the z direction. A polar coordinate system is defined by $x = r\cos\theta$ and $y = r\sin\theta$. The inner and outer faces at $r = a, b$ are traction-free. There are four electrodes at $r = a, c, c + h, b$. The electrodes at $r = c$ and $r = c + h$ are grounded as a reference.

Usually, time-harmonic driving voltage V_1 is applied across the electrodes at $r = b, c + h$. Due to the particular material orientation, the cylinder is driven into axial thickness-shear vibration, and an output voltage V_2 can be picked up across the electrodes at $r = c$, a which are joined by a load circuit whose impedance is Z. In present contribution, we only consider the effect of epoxy layer. Hence, the thickness of the middle layer is small compared with that of piezoelectric input and output portions. If the thickness is considerable, the structure in Fig. 1 can be used to simulate the effect of energy transmission through a wall [24], which will not be discussed in this text. Since the material tensors of crystals of 6 mm symmetry have the same structures as polarized ceramics, our analysis is also valid for 6 mm piezoelectric crystals. This includes widely used materials like ZnO and AlN [25,26].

The displacement vector $\boldsymbol{u}$ and electrical potential function φ of axial thickness-shear modes which belongs to anti-plane or shear horizontal (SH) motions can be described as [27]

$$u_x = u_y = 0, \quad u_z = u(x, y, t) = u(r, \theta, t), \quad \varphi = \varphi(x, y, t) = \varphi(r, \theta, t). \tag{1}$$

Considering the axisymmetric motions independent of θ, which means $u_z = u(r, t)$ and $\varphi = \varphi(r, t)$ [24,28], $\nabla^2 = \frac{\partial^2}{\partial r^2} + \frac{1}{r}\frac{\partial}{\partial r}$ can be obtained. For harmonic motions we use the complex notation

$$[u, \varphi, T_{rz}, D_r, I_1, V_1, Q_1, I_2, V_2, Q_2] = \mathrm{Re}\left\{\left(U, \Phi, T, D, \bar{I}_1, \bar{V}_1, \bar{Q}_1, \bar{I}_2, \bar{V}_2, \bar{Q}_2\right)\exp(i\omega t)\right\}. \tag{2}$$

So the governing equations can be obtained for the piezoelectric materials occupying $a < r < c$ and $c + h < r < b$ [24]

$$\left(\frac{\partial^2}{\partial r^2} + \frac{1}{r}\frac{\partial}{\partial r} + \xi^2\right) U = 0, \tag{3a}$$

$$\left(\frac{\partial^2}{\partial r^2} + \frac{1}{r}\frac{\partial}{\partial r}\right) \Psi = 0. \tag{3b}$$

Where the wavenumber satisfies $\xi = \frac{\omega}{\sqrt{\bar{c}_{44}/\rho_0}}$ with the effective piezoelectric stiffness $\bar{c}_{44} = c_{44} + \frac{e_{15}^2}{\varepsilon_{11}}$, and the auxiliary function is $\Psi = \Phi - \frac{e_{15}}{\varepsilon_{11}}U$ [29]. $c_{44}, e_{15}, \varepsilon_{11}$ and ρ_0 stand for the elastic constant, piezoelectric, dielectric permittivity coefficients and mass density of the piezoelectric material, respectively. Meanwhile, the governing equation of the elastic middle layer occupying $c < r < c + h$ is

$$\left(\frac{\partial^2}{\partial r^2} + \frac{1}{r}\frac{\partial}{\partial r} + \zeta^2\right) U = 0. \tag{4}$$

In which the wavenumber satisfies $\zeta = \frac{\omega}{\sqrt{\mu/\rho}}$. μ and ρ are the elastic constant and mass density of the epoxy-bonded layer.

The corresponding boundary and continuity conditions are

$$r = a : T(a) = 0, \Phi(a) = \bar{V}_2. \tag{5a}$$

$$r = c : T(c^+) = T(c^-), U(c^+) = U(c^-), \Phi(c) = 0. \tag{5b}$$

$$r = c + h : T\left[(c+h)^+\right] = T\left[(c+h)^-\right], U\left[(c+h)^+\right] = U\left[(c+h)^-\right], \Phi(c+h) = 0. \tag{5c}$$

$$r = b : T(b) = 0, \quad \Phi(b) = \bar{V}_1. \tag{5d}$$

The solutions can be obtained as follows [24]

$$U = \begin{cases} A_1 J_0(\xi r) + A_2 Y_0(\xi r), & a < r < c \\ C_1 J_0(\zeta r) + C_2 Y_0(\zeta r), & c < r < c + h \\ B_1 J_0(\xi r) + B_2 Y_0(\xi r), & c + h < r < b \end{cases} \tag{6a}$$

$$\Phi = \begin{cases} \dfrac{e_{15}}{\varepsilon_{11}} \left[A_1 J_0(\xi r) + A_2 Y_0(\xi r)\right] + A_3 \ln r + A_4, & a < r < c \\ 0, & c < r < c + h \\ \dfrac{e_{15}}{\varepsilon_{11}} \left[B_1 J_0(\xi r) + B_2 Y_0(\xi r)\right] + B_3 \ln r + B_4, & c + h < r < b \end{cases} \tag{6b}$$

$$T = \begin{cases} -\bar{c}_{44}\xi \left[A_1 J_1(\xi r) + A_2 Y_1(\xi r)\right] + e_{15}\dfrac{A_3}{r}, & a < r < c \\ -\mu\zeta \left[C_1 J_1(\zeta r) + C_2 Y_1(\zeta r)\right], & c < r < c + h \\ -\bar{c}_{44}\xi \left[B_1 J_1(\xi r) + B_2 Y_1(\xi r)\right] + e_{15}\dfrac{B_3}{r}, & c + h < r < b \end{cases} \tag{6c}$$

$$D = \begin{cases} -\varepsilon_{11}\dfrac{A_3}{r}, & a < r < c \\ 0, & c < r < c + h \\ -\varepsilon_{11}\dfrac{B_3}{r}, & c + h < r < b \end{cases} \tag{6d}$$

Where J_0 and Y_0 are zero-order Bessel functions of the first and second kind. A_1, A_2, A_3, A_4, C_1, C_2, B_1, B_2, B_3 and B_4 are undermined coefficients. Substituting Eq. (6) into Eq. (5) gives

$$\begin{cases} -\bar{c}_{44}\xi \left[A_1 J_1(\xi a) + A_2 Y_1(\xi a)\right] + e_{15}\dfrac{A_3}{a} = 0, \\ \dfrac{e_{15}}{\varepsilon_{11}} \left[A_1 J_0(\xi a) + A_2 Y_0(\xi a)\right] + A_3 \ln a + A_4 = \bar{V}_2. \end{cases} \tag{7a}$$

$$\begin{cases} -\bar{c}_{44}\xi \left[A_1 J_1(\xi c) + A_2 Y_1(\xi c)\right] + e_{15}\dfrac{A_3}{c} = -\mu\zeta \left[C_1 J_1(\zeta c) + C_2 Y_1(\zeta c)\right], \\ A_1 J_0(\xi c) + A_2 Y_0(\xi c) = C_1 J_0(\zeta c) + C_2 Y_0(\zeta c), \\ \dfrac{e_{15}}{\varepsilon_{11}} \left[A_1 J_0(\xi c) + A_2 Y_0(\xi c)\right] + A_3 \ln c + A_4 = 0. \end{cases} \tag{7b}$$

$$\begin{cases} -\bar{c}_{44}\xi\left[B_1J_1(\xi c+\xi h)+B_2Y_1(\xi c+\xi h)\right]+e_{15}\dfrac{B_3}{c+h}=-\mu\zeta\left[C_1J_1(\zeta c+\zeta h)+C_2Y_1(\zeta c+\zeta h)\right], \\ B_1J_0(\xi c+\xi h)+B_2Y_0(\xi c+\xi h)=C_1J_0(\zeta c+\zeta h)+C_2Y_0(\zeta c+\zeta h), \\ \dfrac{e_{15}}{\varepsilon_{11}}\left[B_1J_0(\xi c+\xi h)+B_2Y_0(\xi c+\xi h)\right]+B_3\ln(c+h)+B_4=0. \end{cases} \tag{7c}$$

$$\begin{cases} -\bar{c}_{44}\xi\left[B_1J_1(\xi b)+B_2Y_1(\xi b)\right]+e_{15}\dfrac{B_3}{b}=0, \\ \dfrac{e_{15}}{\varepsilon_{11}}\left[B_1J_0(\xi b)+B_2Y_0(\xi b)\right]+B_3\ln b+B_4=\bar{V}_1. \end{cases} \tag{7d}$$

Formally, Eq. (7) contains ten equations for $A_1, A_2, A_3, A_4, C_1, C_2, B_1, B_2, B_3$ and B_4, but the output voltage $\bar{V}_2$ is unknown. The additional equation needed is the output circuit. The charge can be obtained at $r = a$:

$$\bar{Q}_2=\int_0^{2\pi} D|_{r=a}ad\theta=-2\pi\varepsilon_{11}A_3. \tag{8}$$

Owning to the fact $I_2=-\dot{Q}_2$, the relationship between the complex output voltage and current can be written as

$$\bar{V}_2=\bar{I}_2Z=2\pi i\omega\varepsilon_{11}ZA_3. \tag{9}$$

Equations (7) and (9) contain eleven equations with eleven undetermined coefficients A_1, A_2, A_3, A_4, C_1, C_2, B_1, B_2, B_3, B_4 and $\bar{V}_2$, by which the output voltage ratio $m=\left|\bar{V}_2/\bar{V}_1\right|$ can be calculated easily by MATLAB software. Similarly with output voltage and current, $I_1=\dot{Q}_1$ can be easily obtained at $r = b$, and the input current satisfied

$$\bar{I}_1=i\omega\int_0^{2\pi}-D|_{r=b}bd\theta=2\pi i\omega\varepsilon_{11}B_3. \tag{10}$$

With the complex notation for harmonic motions, the input electrical power is given by

$$P_1=\frac{1}{4}\left(\bar{I}_1\bar{V}_1^*+\bar{I}_1^*\bar{V}_1\right), \tag{11}$$

where an asterisk represents complex conjugate. Meanwhile, the input admittance is

$$S_1=\left|\bar{I}_1/\bar{V}_1\right|. \tag{12}$$

Similarly, the output electrical power is

$$P_2=\frac{1}{4}(\bar{I}_2\bar{V}_2^*+\bar{I}_2^*\bar{V}_2). \tag{13}$$

The efficiency of the transformer is defined as

$$\eta=P_2/P_1. \tag{14}$$

Another quantity of practical interest is the power per unit volume (power density). In Fig. 1, z direction is infinite. During the following discussion, we assumed that the thickness is one unit. Hence, p_2 has the dimensional of W/m^2, which in our case may be calculated from

$$p_2=\frac{P_2}{\pi a^2}. \tag{15}$$

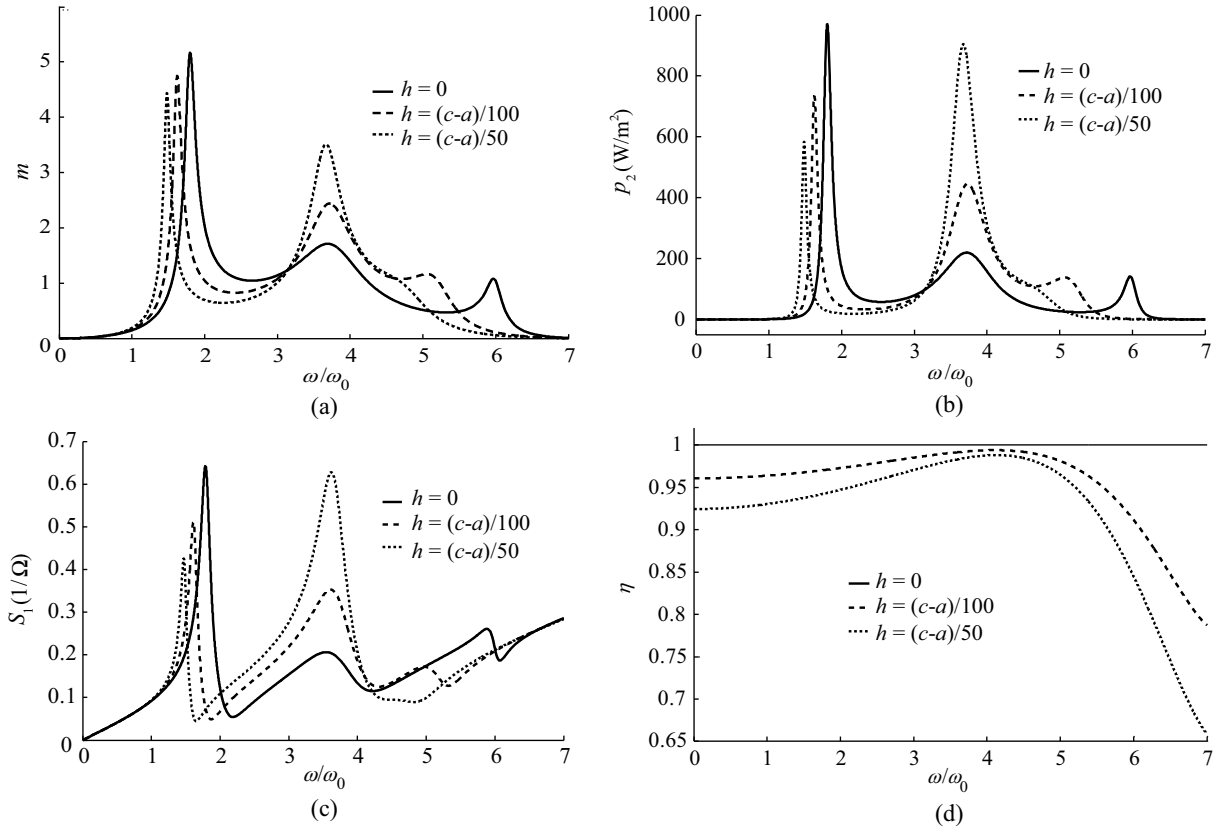

Fig. 2. The first three resonances of the (a) transforming ratio m, (b) power density p_2, (c) admittance S_1 and (d) efficiency η versus the driving frequency for some selected h.

3. The effect of the epoxy-bonded layer on the transformer

As a numerical example, consider a ceramic cylinder of PZT-5H with $c_{44} = 2.3 \times 10^{10}$ N/m^2, $e_{15} =$ 17 C/m^2, $\varepsilon_{11} = 1.506 \times 10^{-8}$ F/m, and $\rho_0 = 7500$ kg/m^3 [28,30]. However, the characteristics of the epoxy-bonded layer, such as the elastic constant and the density, can not be obtained directly. The inverse method with the help of experimental data can be used to determine the properties of this thin layer using laser-generated Love surface waves [22] or Rayleigh waves [9,23]. In present paper, we adopt the material coefficient as follows: $\mu = 1.3117 \times 10^9$ N/m^2 and $\rho = 1150$ kg/m^3, which has been verified by experiment in Ref. [23].

Considering the viscous damping, in our calculations μ is replaced by $\mu\,(1+ iQ^{-1})$, where Q is a large and real number with the magnitude order of 10^2 to 10^3. We fixed $Q = 100$. $a = 10$ mm, $c = 20$ mm, $b = c + h + c - a$. Meanwhile, the fundamental thickness-shear frequency of shell $\omega_0 = \frac{\pi}{2(b-a)}\sqrt{\frac{\bar{c}_{44}}{\rho}}$, impedance $Z_0 = \frac{1}{i\omega C_0}$, and static capacitance $C_0 = \frac{2\pi\varepsilon_{11}}{\ln(b/c)}$ are introduced for convenience [24,28]. The additional load is fixed as $Z = (1-i)Z_0$ during the following simulation.

In this text, we mainly focus on the effect of the properties of epoxy-bonded layer on the transformer, including the thickness, elastic coefficient and mass density. Here we assume that the elastic coefficient and mass density of the thin layer are homogeneous when we focus on the effect of the thickness, and the same method can be used to deal with the elastic coefficient and mass density.

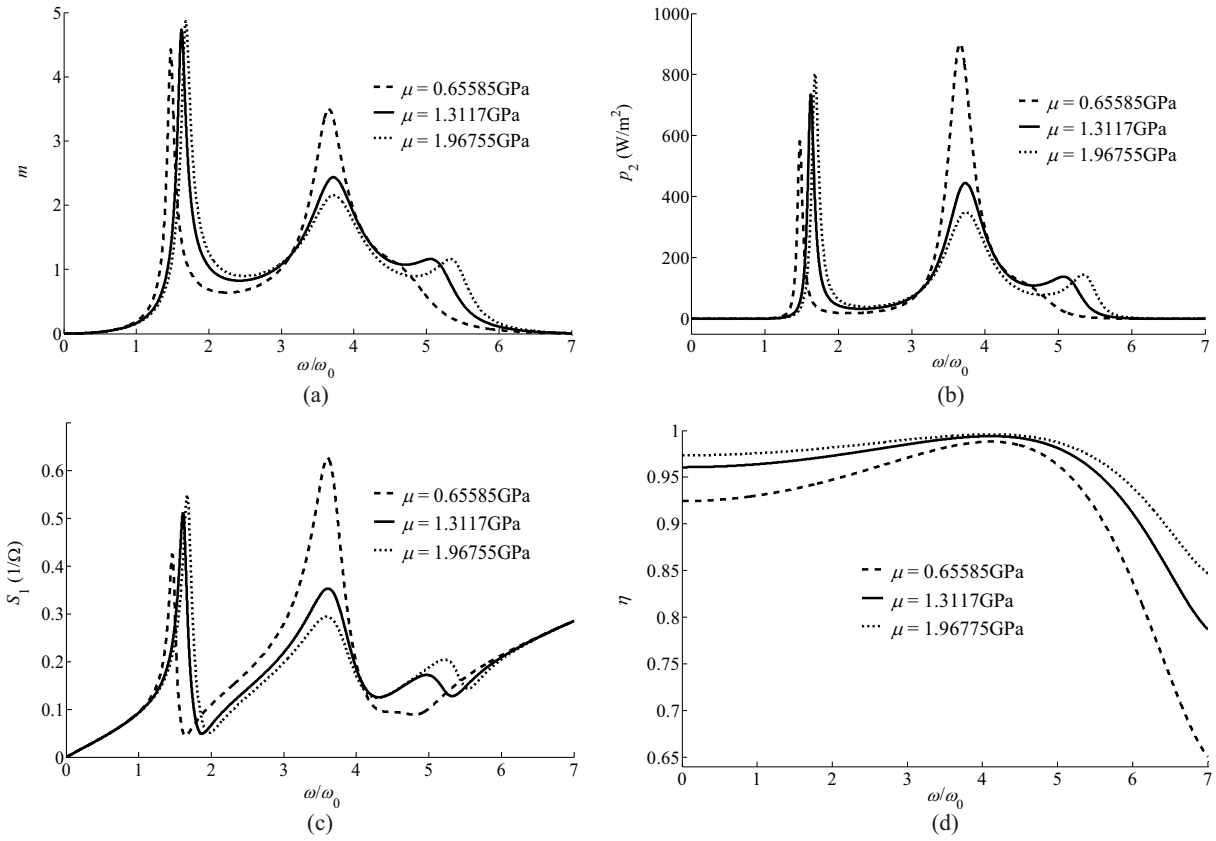

Fig. 3. The first few resonances of the (a) transforming ratio m,(b) power density p_2, (c) admittance S_1 and (d) efficiency η versus the driving frequency for some selected μ when the thickness of epoxy-bonded layer $h = (c - a)/100$.

Figures 2(a)–(d) respectively show the first three resonances of the transforming ratio m, power density p_2, admittance S_1 and efficiency η versus the driving frequency for some selected h. It can be seen from Fig. 2 that the transforming ratio assumes its maxima at resonant frequencies as expected. Meanwhile, at the same resonances the input admittance and output energy flux also assume their maxima, which means the transformer is a resonant device operating at a particular frequency [24,28]. When there is no epoxy-bonded layer, the first resonance has the highest transforming ratio, output energy flux and input admittance, which owns to the fact that the higher corresponding modes have nodal points and some voltage cancellation usually occurs along the radius direction [1,24,28]. However, the thickness h changes its performance. The increasing thickness lowers both the first resonance frequency and magnitude of these values. For the second modes, the peak value of m, p_2 and S_1 raise with the increasing thickness. To the pointed, the efficiency η is equal to unit and keeps constant versus the driving frequency when $h = 0$. The viscous damping depends directly on the elastic coefficient of the epoxy-bonded layer. Hence, no viscous damping consumes at the circumstance of no thin layer. Totally, the thickness of the epoxy-bonded layer has a great influence on the behavior of the transformer.

To demonstrate more closely the effect of the soft middle layer, Figs 3(a)–(d) respectively plot the first three resonances of the transforming ratio m, power density p_2, admittance S_1 and efficiency η versus the driving frequency for some selected μ. Here, we assumed that the thickness of epoxy-bonded layer is $h = (c - a)/100$, and the elastic coefficient μ changes from -50% to 50% of the initial value. The

Table 1
The values of transforming ratio m, power density p_2, admittance S_1 and efficiency η for the first three resonance frequencies when the density of epoxy-bonded layer shifts

	ρ (kg/m^3)	m	p_2 (W/m^2)	S_1(1/Ω)	η
$\omega = 1.623\omega_0$	575	4.73790	733.59719	0.49789	0.96896
	862.5	4.73891	733.90865	0.49798	0.96896
	1150	4.73991	734.21927	0.49807	0.96895
	1437.5	4.74091	734.52904	0.49816	0.96894
	1725	4.74192	734.83797	0.49824	0.96893
$\omega = 3.719\omega_0$	575	2.43650	444.74236	0.33421	0.99250
	862.5	2.43597	444.55376	0.33378	0.99250
	1150	2.43543	444.36112	0.33336	0.99251
	1437.5	2.43488	444.16445	0.33293	0.99251
	1725	2.43701	443.96377	0.33250	0.99252
$\omega = 5.059\omega_0$	575	1.16233	137.62328	0.16783	0.97936
	862.5	1.16252	137.66725	0.16788	0.97935
	1150	1.16270	137.71127	0.16794	0.97934
	1437.5	1.16289	137.75532	0.16800	0.97933
	1725	1.16308	137.79941	0.16805	0.97932

tendency of these curves is similar with Fig. 2 except for the energy efficiency η. Larger μ leads to more energy dissipation and then lowers energy efficiency. The elastic coefficient of the epoxy-bonded layer also makes a big difference on the performance of the transformer. To the pointed, this kind of effect is based on the fact that the thickness of the middle layer is not zero. If there does not exist the epoxy-bonded layer, the influence is also null.

The first three peak values of the transforming ratio m, power density p_2, admittance S_1 and efficiency η when the mass density shifts from -50% to 50% are shown in Table 1. It is clear from these results that the mass density of the epoxy layer has a negligible influence on the performance in the present structure.

4. A cylindrical piezoelectric ceramic transformer with an imperfect interface

Consider next a structure consisting of two transversely piezoelectric layers, the input ceramics and output one occupying the regions $c < r < b$ and $a < r < c$ respectively, with the interface imperfectly bonded, as shown in Fig. 4. The solutions for thickness-shear modes in the regions have already been given in Eq. (6) by the present epoxy-bonded layer structure. Here, alternative solutions are exploited by applying the shear-lag model. The predictions from the two different models will be compared in the next section using theoretical analysis and numerical examples.

The boundary conditions in Fig. 4 at $r = a$ and $r = b$ are the same as Eqs (5a) and (5b), and the additional output circuit condition is just Eq. (8). For simplicity and as an approximation, the interface may be characterized using the shear-lag model, i.e., its tangential displacement is allowed to be different from both sides of the interface [12,13,15,16]. For the imperfectly bonded interface $r = c$ as shown in Fig. 4, the shear-lag model dictates that:

$$r = c : T(c^+) = T(c^-) = K\left[U(c^+) - U(c^-)\right], \Phi(c^+) = \Phi(c^-) = 0. \tag{16}$$

Where K (N/m^3) is the interfacial elastic constant describing how well the interface is bonded, with $K = \infty$ for perfect bonding and $K = 0$ for no bonding. Meanwhile, we use a complex interface stiffness

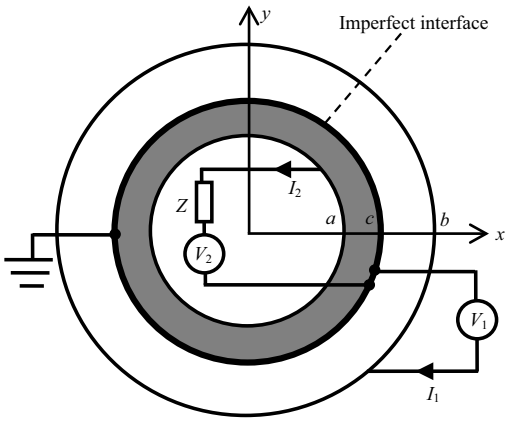

Fig. 4. A cylindrical piezoelectric ceramic transformer with an imperfect interface.

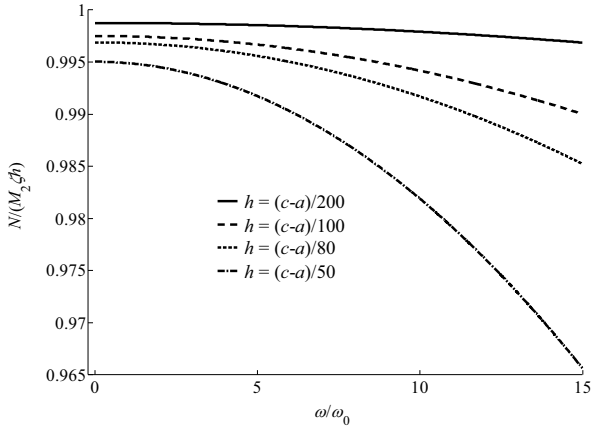

Fig. 5. The values of $\frac{N}{M_2\zeta h}$ versus the driving frequency for some selected h.

whose imaginary part describes interface damping. Consider $K = K_0 + iK_1$, where both K_1 and K_2 are real. Substitution of Eq. (6), into Eqs (5a), (5d), (9) and (16) can lead to nine algebraic equations for the unknown constants $A_1, A_2, A_3, A_4, B_1, B_2, B_3, B_4$ and $\bar{V}_2$, in which the boundary conditions at $r = a$ and $r = b$ are the same as Eqs (7a) and (7b), and the additional output circuit condition is the same as Eq. (9). However, at $r = c$:

$$\begin{cases} -\bar{c}_{44}\xi\left[A_1 J_1(\xi c) + A_2 Y_1(\xi c)\right] + e_{15}\dfrac{A_3}{c} = -\bar{c}_{44}\xi\left[B_1 J_1(\xi c) + B_2 Y_1(\xi c)\right] + e_{15}\dfrac{B_3}{c} \\ = K\left[-A_1 J_0(\xi c) - A_2 Y_0(\xi c) + B_1 J_0(\xi c) + B_2 Y_0(\xi c)\right], \\ \dfrac{e_{15}}{\varepsilon_{11}}\left[A_1 J_0(\xi c) + A_2 Y_0(\xi c)\right] + A_3 \ln c + A_4 = 0, \\ \dfrac{e_{15}}{\varepsilon_{11}}\left[B_1 J_0(\xi c) + B_2 Y_0(\xi c)\right] + B_3 \ln c + B_4 = 0. \end{cases} \tag{17}$$

If the interface is perfect, i.e., $K = \infty$, Eqs (7a), (7d), (9) and (17) possess exactly the same expressions obtained in the work by Yang [28], which validates to some extent the accuracy of the theoretical derivation. Furthermore, these equations mentioned above can be simplified as

$$\begin{aligned} &\left\{k_e^2\left[J_0(\xi a) - J_0(\xi c)\right] + a\xi \ln\left(\frac{a}{c}\right) J_1(\xi a)\left(1 - \frac{Z}{Z_0}\right)\right\} A_1 \\ &\quad + \left\{k_e^2\left[Y_0(\xi a) - Y_0(\xi c)\right] + a\xi \ln\left(\frac{a}{c}\right) Y_1(\xi a)\left(1 - \frac{Z}{Z_0}\right)\right\} A_2 = 0, \end{aligned} \tag{18a}$$

$$\begin{aligned} &-\left[\frac{a}{c}J_1(\xi a) - J_1(\xi c)\right] A_1 - \left[\frac{a}{c}Y_1(\xi a) - Y_1(\xi c)\right] A_2 \\ &\quad + \left[\frac{b}{c}J_1(\xi b) - J_1(\xi c)\right] B_1 + \left[\frac{b}{c}Y_1(\xi b) - Y_1(\xi c)\right] B_2 = 0, \end{aligned} \tag{18b}$$

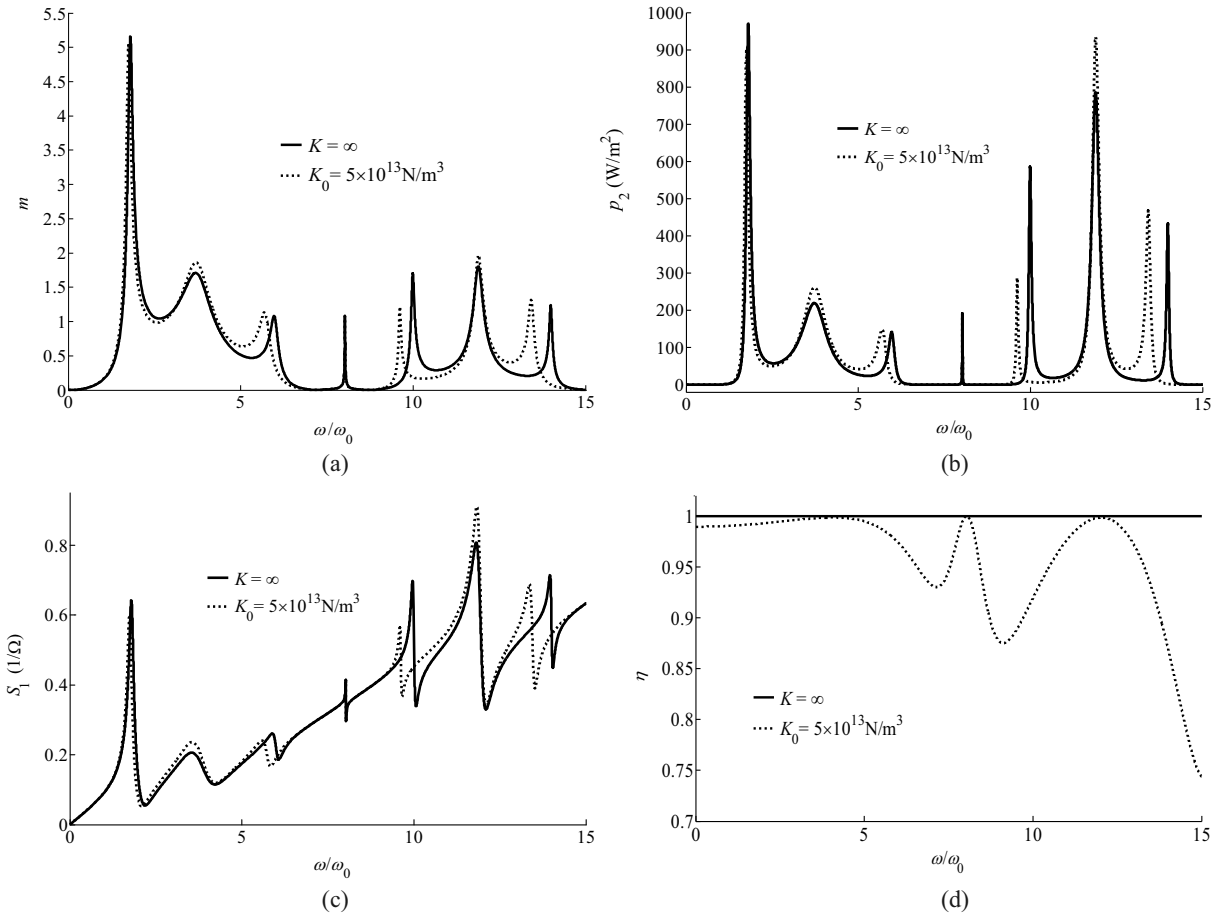

Fig. 6. The first few resonances of the (a) transforming ratio m, (b) power density p_2, (c) admittance S_1 and (d) efficiency η versus the driving frequency for the perfect and imperfect interfaces.

$$-\left\{J_0(\xi c)+\frac{\bar{c}_{44}\xi}{K}\left[\frac{a}{c}J_1(\xi a)-J_1(\xi c)\right]\right\}A_1-\left\{Y_0(\xi c)+\frac{\bar{c}_{44}\xi}{K}\left[\frac{a}{c}Y_1(\xi a)-Y_1(\xi c)\right]\right\}A_2 +J_0(\xi c)B_1+Y_0(\xi c)B_2=0, \tag{18c}$$

$$\left\{k_e^2\left[J_0\left(\xi b\right)-J_0\left(\xi c\right)\right]+b\xi\ln\left(\frac{b}{c}\right)J_1\left(\xi b\right)\right\}B_1 +\left\{k_e^2\left[Y_0\left(\xi b\right)-Y_0\left(\xi c\right)\right]+b\xi\ln\left(\frac{b}{c}\right)Y_1\left(\xi b\right)\right\}B_2=\frac{e_{15}}{\bar{c}_{44}}\bar{V}_1. \tag{18d}$$

Where $k_e^2=\frac{e_{15}^2}{\varepsilon_{11}\bar{c}_{44}}$ is the electromechanical coupling constant. Equation (18) can be used to solve A_1, A_2, B_1 and B_2. Once they are solved, the output voltage ratio $\left|\bar{V}_2/\bar{V}_1\right|$ can be obtained.

In order to compare Figs 1 and 4, Eqs (7) and (9) also can be reduced as the expression about

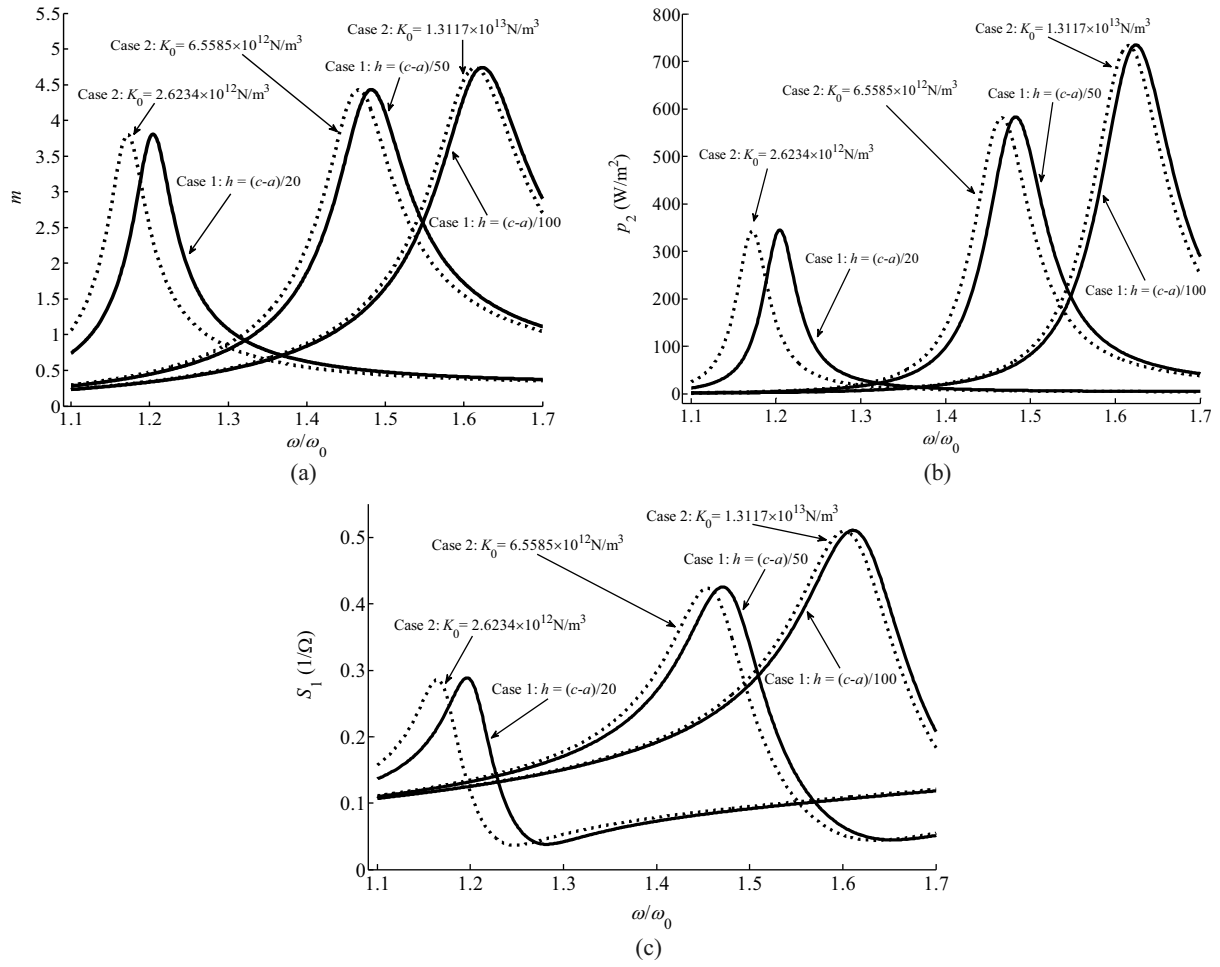

Fig. 7. The comparison between the epoxy layer structure and shear-lag model for the first resonance of the (a) transforming ratio m, (b) power density p_2 and (c) admittance S_1 when the thickness of epoxy-bonded layer shifts.

A_1, A_2, B_1 and B_2 as follows:

$$\left\{k_e^2\left[J_0\left(\xi a\right)-J_0\left(\xi c\right)\right]+a\xi\ln\left(\frac{a}{c}\right)J_1\left(\xi a\right)\left(1-\frac{Z}{Z_0}\right)\right\}A_1 + \left\{k_e^2\left[Y_0\left(\xi a\right)-Y_0\left(\xi c\right)\right]+a\xi\ln\left(\frac{a}{c}\right)Y_1\left(\xi a\right)\left(1-\frac{Z}{Z_0}\right)\right\}A_2=0, \tag{19a}$$

$$\left\{-M\left[\frac{a}{c}J_1(\xi a)-J_1(\xi c)\right]+\frac{\mu\zeta}{\bar{c}_{44}\xi}\frac{J_0(\xi c)}{J_0(\zeta c)}\left[J_1(\zeta c+\zeta h)-MJ_1(\zeta c)\right]\right\}A_1 + \left\{-M\left[\frac{a}{c}Y_1(\xi a)-Y_1(\xi c)\right]+\frac{\mu\zeta}{\bar{c}_{44}\xi}\frac{Y_0(\xi c)}{J_0(\zeta c)}\left[J_1(\zeta c+\zeta h)-MJ_1(\zeta c)\right]\right\}A_2 + \left[\frac{b}{c+h}J_1(\xi b)-J_1(\xi c+\xi h)\right]B_1+\left[\frac{b}{c+h}Y_1(\xi b)-Y_1(\xi c+\xi h)\right]B_2=0, \tag{19b}$$

Table 2
The comparison between the epoxy layer structure and shear-lag model for the first resonance of the efficiency η when the thickness of epoxy-bonded layer shifts

ω/ω_0	1.1	1.3	1.5	1.7
Case 1: $h=(c-a)/20$	0.84513	0.85085	0.85737	0.86495
Case 2: $K_0=2.6234\times10^{12}$ N/m^3	0.84496	0.85075	0.85746	0.86506
Case 1: $h=(c-a)/50$	0.93161	0.93439	0.93758	0.94116
Case 2: $K_0=6.5585\times10^{12}$ N/m^3	0.93162	0.93443	0.93765	0.94127
Case 1: $h=(c-a)/100$	0.96459	0.96609	0.9678	0.96971
Case 2: $K_0=1.3117\times10^{13}$ N/m^3	0.9646	0.9661	0.96782	0.96975

Table 3
The comparison between the epoxy layer structure and shear-lag model for the first resonance of the efficiency η when the elastic coefficient of epoxy-bonded layer shifts and $h=(c-a)/100$

ω/ω_0	1.3	1.5	1.7	1.9
Case 1: $\mu=0.65585$ GPa	0.93441	0.93761	0.94121	0.94517
Case 2: $K_0=6.5585\times10^{12}$N/m^3	0.93443	0.93765	0.94127	0.9718
Case 1: $\mu=1.3117$ GPa	0.96609	0.9678	0.96971	0.9718
Case 2: $K_0=1.3117\times10^{13}$ N/m^3	0.9661	0.96782	0.96975	0.97186
Case 1: $\mu=1.96755$ GPa	0.97713	0.9783	0.9796	0.98102
Case 2: $K_0=1.96755\times10^{13}$ N/m^3	0.97714	0.97832	0.97963	0.98106

$$
\begin{aligned}
&-\left\{J_0(\zeta c+\zeta h)\frac{J_0(\xi c)}{J_0(\zeta c)}+\frac{\bar{c}_{44}\xi}{\mu/h}\frac{N}{M_2\zeta h}\left[\frac{a}{c}J_1(\xi a)-J_1(\xi c)\right]-J_1(\zeta c)\frac{J_0(\xi c)}{J_0(\zeta c)}\frac{N}{M_2}\right\}A_1\\
&\quad-\left\{J_0(\zeta c+\zeta h)\frac{Y_0(\xi c)}{J_0(\zeta c)}+\frac{\bar{c}_{44}\xi}{\mu/h}\frac{N}{M_2\zeta h}\left[\frac{a}{c}Y_1(\xi a)-Y_1(\xi c)\right]-J_1(\zeta c)\frac{Y_0(\xi c)}{J_0(\zeta c)}\frac{N}{M_2}\right\}A_2\\
&\quad+J_0(\xi c+\xi h)B_1+Y_0(\xi c+\xi h)B_2=0,
\end{aligned}
\tag{19c}
$$

$$
\begin{aligned}
&\left\{k_e^2\left[J_0\left(\xi b\right)-J_0\left(\xi c+\xi h\right)\right]+b\xi\ln\left(\frac{b}{c+h}\right)J_1\left(\xi b\right)\right\}B_1\\
&\quad+\left\{k_e^2\left[Y_0\left(\xi b\right)-Y_0\left(\xi c+\xi h\right)\right]+b\xi\ln\left(\frac{b}{c+h}\right)Y_1\left(\xi b\right)\right\}B_2=\frac{e_{15}}{\bar{c}_{44}}\bar{V}_1.
\end{aligned}
\tag{19d}
$$

Where

$$
\begin{cases}
M=\dfrac{M_1}{M_2}=\dfrac{J_1(\zeta c+\zeta h)\dfrac{Y_0(\zeta c)}{J_0(\zeta c)}-Y_1(\zeta c+\zeta h)}{J_1(\zeta c)\dfrac{Y_0(\zeta c)}{J_0(\zeta c)}-Y_1(\zeta c)},\\[2ex]
N=Y_0(\zeta c+\zeta h)-J_0(\zeta c+\zeta h)\dfrac{Y_0(\zeta c)}{J_0(\zeta c)}.
\end{cases}
\tag{20}
$$

Upon comparing Eqs (18) and (19), one may conclude that when the thickness of the epoxy-bonded layer are diminishingly small, i.e., $h\to0$, $N\to0$ and $M\to1$ can be obtained. Based on the fact that $\frac{N}{M_2\zeta h}\to1$ for thin middle layer (Fig. 5), if $K=\mu/h$ is assumed, Eqs (18) and (19) have the same expression. Under such conditions, in addition to the description of the shear-lag model, the imperfect

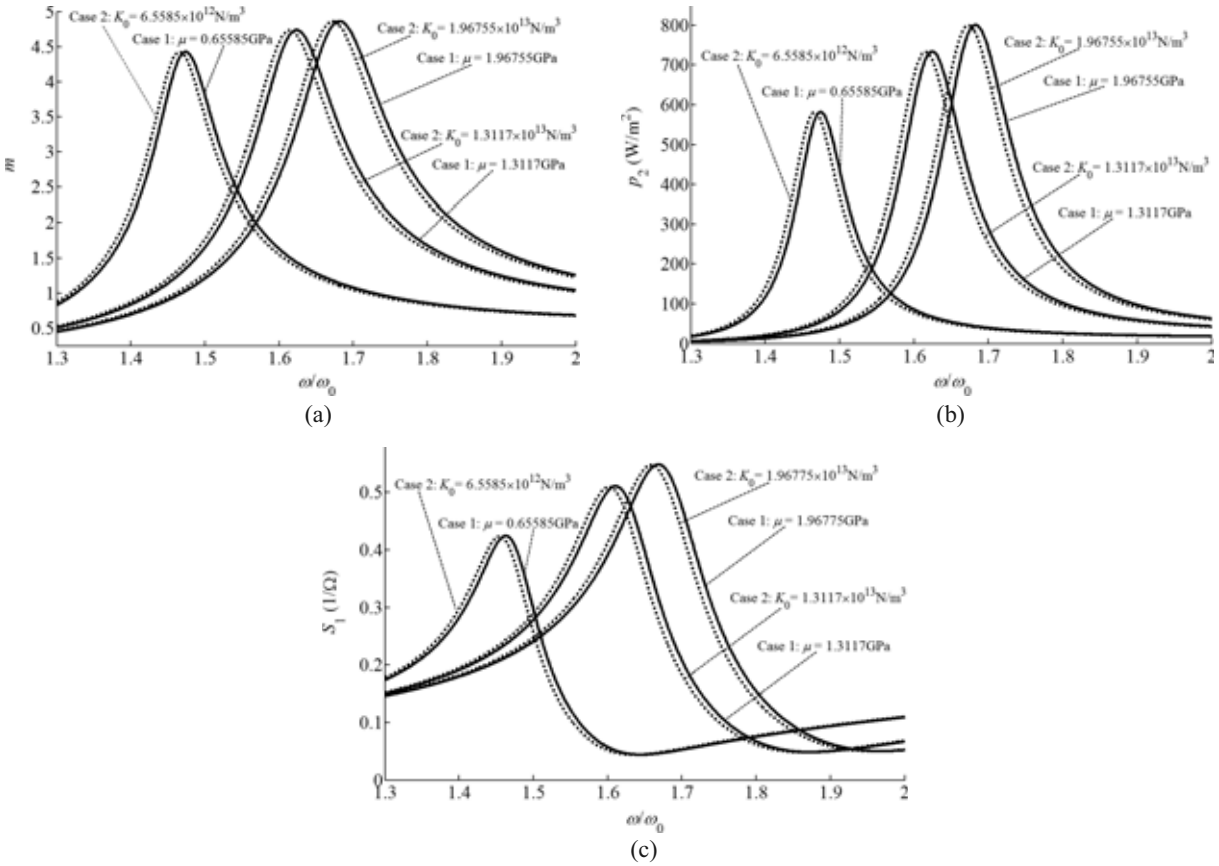

Fig. 8. The comparison between the epoxy layer structure and shear-lag model for the first resonance of the (a) transforming ratio m, (b) power density p_2 and (c) admittance S_1 when the elastic coefficient of epoxy-bonded layer shifts and $h = (c - a)/100$.

interface may be regarded as an epoxy-bonded layer and hence the solutions obtained in the previous sections apply. Therefore, we can conclude that the interface viscous damping absolutely comes from the viscoelasticity, i.e., the elastic coefficient of the epoxy-bonded layer.

$$K = K_0 + iK_1 = \frac{\mu(1 + iQ^{-1})}{h} = \frac{\mu}{h} + i\frac{\mu Q^{-1}}{h} \tag{21}$$

Meanwhile, if $h \to \infty$, K approaches zero, which is the case of no bonding. Equation (21) provides a theoretical relationship between the epoxy-bonded layer structure and shear-lag model. Figures 6(a)–(d) respectively show the first few resonances of the transforming ratio m, power density p_2, admittance S_1 and efficiency η versus the driving frequency for the perfect and imperfect interfaces using the shear-lag model. These curves have the same varying patterns as Fig. 2, which corrects our theoretical analysis from the point of numerical simulations.

Figure 7 presents the comparison between the epoxy-bonded layer structure and shear-lag model for the first resonance of the transforming ratio m, power density p_2 and admittance S_1 when the thickness of epoxy-bonded layer shifts. Case 1 is the outcomes calculated by the epoxy-bonded layer structure, i.e., Eq. (19), and Case 2 is the corresponding shear-lag results at the same interface conditions, i.e., Eq. (18). Meanwhile, the comparison results about the energy efficient η are shown in Table 2. It is seen

from Fig. 7 and Table 2 that the difference between the two cases is evident. Especially when the epoxy layer is relatively large, the calculation by the shear-lag model will leads to deviation, which must be noticed in the device application. To a certain degree, this kind of error can be explained by the value of $\frac{N}{M_2\zeta h}$ in Fig. 5. For larger h, this value does not approach to unit any more.

Similarly, Fig. 8 and Table 3 simultaneously provide the comparison between the epoxy-bonded layer structure and shear-lag model of the first resonance of the transforming ratio m, power density p_2, admittance S_1 and efficient η for fixed thickness $h = (c-a)/100$ when the elastic coefficient of epoxy-bonded layer μ shifts. At this condition, the difference between the two cases is also evident. However, this deviation calculated by the shear-lag model will not be enlarged with the changing of the elastic coefficient of epoxy-bonded layer.

5. Conclusion

The presence of an epoxy-bonded layer and its influence on the performance of the piezoelectric transformers has been investigated theoretically and numerically from the equations of the linear theory of piezoelectricity. Systematic parametric studies are carried out to quantify the effects of the epoxy-bonded layer, including its thickness, elastic coefficient and mass density. The proposed epoxy-bonded layer structure is also employed to investigate the influence of imperfectly bonded interface in the piezoelectric transformer and the predictions are compared with those obtained using the traditional shear-lag model. The following conclusions are drawn:

(1) The thickness and elastic coefficient of the epoxy-bonded layer affect significantly the properties of the piezoelectric transformer, including its resonance frequencies, transforming ratio, power density, admittance and efficiency, whilst the mass density has negligible influence.
(2) For the piezoelectric transformer with an imperfectly bonded interface between the input and output portions, the calculated results obtained from the epoxy-bonded layer structure has the same expression as that from the shear-lag model if the thickness of the middle layer approaches zero, which means that the imperfect interface may be modeled as a thin epoxy-bonded layer.
(3) The interface coefficient in the shear-lag model is equal to the elastic coefficient divided by the thickness of the epoxy-bonded layer, which explains to certain degree that the interface viscous damping absolutely comes from the viscoelasticity, i.e., the elastic coefficient.
(4) For imperfectly bonded piezoelectric transformers, the predictions considering the present epoxy-bonded layer are more accurate than those from the shear-lag model especially when the thickness of the middle layer is not relatively small.

The theoretical and numerical results can provide guidance in the design of circular cylinder piezoelectric transformer when an imperfect interface appears, especially for the small smart piezoelectric devices with only several micro-meters thick.

Acknowledgment

The National Natural Science Foundation of China (No. 11272247) and the National 111 Project of China (No. B06024) are gratefully acknowledged for their financial support.

References

[1] J.S. Yang and Z.T. Yang, Analytical and numerical modeling of resonant piezoelectric devices in China-a review, *Science in China Series G: Physics, Mechanics & Astronomy* **51** (2008), 1775–1807.

[2] Z.T. Yang, J.S. Yang and Y.T. Hu, Electrically forced shear horizontal vibration of a circular cylindrical elastic shell with a finite piezoelectric actuator, *Archive of Applied Mechanics* **79** (2009), 955–964.

[3] J.S. Yang, S.N. Jiang and Y.T. Hu, Analysis of rosen piezoelectric transformers with end masses, *International Journal of Applied Electromagnetics and Mechanics* **32** (2010), 97–110.

[4] V.L. Karlash, Electroelastic vibrations and transformation ratio of a planar piezoceramic transformer, *Journal of Sound and Vibration* **277** (2004), 353–367.

[5] Y.H. Hsu, C.H. Lee and W.H. Hsiao, Optimizing piezoelectric transformer for maximum power transfer, *Smart Materials and Structures* **12** (2003), 373–383.

[6] L. Hwang, J. Yoo, E. Jang, D. Oh, Y. Jeong, I. Ahn and M. Cho, Fabrication and characteristics of PDA LCD backlight driving circuits using piezoelectric transformer, *Sensors and Actuators A: Physical* **115** (2004), 73–78.

[7] S. Katsutoshi, N. Tohru, S. Sigeru, O. Kazumasa and T. Yoshiro, Experimental investigation of a piezoelectric ceramic transformer using radial vibration of disks combined with a coupling element, *Japanese Journal of Applied Physics* **37** (1998), 2896–2900.

[8] J.S. Yang, Piezoelectric transformer structural modeling-a review, *IEEE Transactions on Ultrasonics, Ferroelectrics, and Frequency Control* **54** (2007), 1154–1170.

[9] T.-T. Wu and Y.-H. Liu, Inverse determinations of thickness and elastic properties of a bonding layer using laser-generated surface waves, *Ultrasonics* **37**(1999), 23–30.

[10] X.S. Cao, F. Jin and I. Jeon, Rayleigh surface wave in a piezoelectric wafer with subsurface damage, *Applied Physics Letters* **95** (2009), 261906.

[11] H.M. Shodja, S.M. Tabatabaei and M.T. Kamali, A piezoelectric-inhomogeneity system with imperfect interface, *International Journal of Engineering Science* **44** (2006), 291–311.

[12] W.Q. Chen and K.Y. Lee, Exact solution of angle-ply piezoelectric laminates in cylindrical bending with interfacial imperfections, *Composite Structures* **65** (2004), 329–337.

[13] A. Melkumyan and Y.W. Mai, Influence of imperfect bonding on interface waves guided by piezoelectric/piezomagnetic composites, *Philosophical Magazine* **88** (2008), 2965–2977.

[14] G.S. Murtya, A theoretical model for the attenuation and dispersion of stoneley waves at the loosely bonded interface of elastic half space, *Sphysics of the Earth and Planetary Interiors* **11** (1975), 65–79.

[15] S. Leungvichcharoen and A.C. Wijeyewickrema, Dispersion effects of extensional waves in pre-stressed imperfectly bonded incompressible elastic layered composite, *Wave Motion* **38** (2003), 311–325.

[16] G.L. Dybwad, A sensitive new method for the determination of adhesive bonding between a particle and a substrate, *Journal of Applied Physics* **58** (1985), 2789–2790.

[17] F. Jin, K. Kishimoto, H. Inoue and T. Tateno, Experimental investigation on the interface properties evaluation in piezoelectric layered structures by Love waves propagation, *Key Engineering Materials* **297–300** (2005), 807–812.

[18] A.I. Lavrentyev and S.I. Rokhlin, Ultrasonic spectroscopy of imperfect contact interfaces between a layer and two solids, *Journal of the Acoustical Society of America* **103** (1998), 657–664.

[19] Y.S. Wang, G.L. Yu, Z.M. Zhang and Y.D. Feng, Review on elastic waves propagation under complex interface (interface layer) conditions, *Advances in Mechanics*, In Chinese, **30** (2000), 378–389.

[20] P.B. Nagy, Ultrasonic classification of imperfect interfaces, *Journal of Nondestructive Evaluation* **11** (1992), 127–139.

[21] Y. Termonia, Fibre coating as a means to compensate for poor adhesion in fibre-reinforced materials, *Journal of Materials Science* **25** (1990), 103–106.

[22] P. Kielczynski and M. Szalewski, An inverse method for determining the elastic properties of thin layers using Love surface waves, *Inverse Problems in Science and Engineering* **19** (2011), 31–43.

[23] T. -T. Wu and Y. -C. Chen, Dispersion of laser generated surface waves in an epoxy-bonded layered medium, *Ultrasonics* **34** (1996), 793–799.

[24] W.Q. Chen, C.F. Lu, J.S. Yang and J. Wang, A circular cylindrical, radially polarized ceramic shell piezoelectric transformer, *IEEE Transactions on Ultrasonics, Ferroelectrics, and Frequency Control* **56** (2009), 1238–1245.

[25] H.F. Zhang, J.A. Turner and J.A. Kosinski, Analysis of thickness vibrations of *c*-axis inclined aluminum-nitrogen thin film resonators, *Integrated Ferroelectrics* **113** (2009), 95–108.

[26] L.F. Qin, Q.M. Chen, H.B. Cheng and Q.M. Wang, Analytical study of dual-mode thin film bulk acoustic resonators (FBARs) based on ZnO and AlN films with tilted *c*-axis orientation, *IEEE Transactions on Ultrasonics, Ferroelectrics, and Frequency Control* **57** (2010), 1840–1853.

[27] M.Y. Son and Y.J. Kang, Propagation behavior of SH waves in layered piezoelectric plates, *Journal of Mechanical Science and Technology* **25** (2011), 613–619.

[28] J.S. Yang, Z.G. Chen and Y.T. Hu, Theoretical modeling of a thickness-shear mode circular cylinder piezoelectric transformer, *IEEE Transactions on Ultrasonics, Ferroelectrics, and Frequency Control* **54** (2007), 621–626.
[29] R.G. Curtis and M. Redwood, Transverse surface waves on a piezoelectric material carrying a metal layer of finite thickness, *Journal of Applied Physics* **44** (1973), 2002–2007.
[30] L.M. Xu, Y.L. Geng, Y. Zhang and H. Fan, Power transmission through an unbounded elastic plate using a finite piezoelectric actuator and a finite piezoelectric power harvester, *International Journal of Applied Electromagnetics and Mechanics* **29** (2009), 145–156.